J. Earth Planet. Sci. Nagoya Univ., Vol. 55, 23 to 37, 2008

CHIME dating of monazite from the Dongqing pluton in SE Jilin, China

Deyou SUN[1], Kazuhiro SUZUKI[2], Izumi KAJIZUKA[2], Hiroshi KAMIKUBO[3,2], Xiaoping LU[4] and Fuyuan WU[5]

[1]College of Earth Sciences, Jilin University, Changchun 130061, China
[2]The Center for Chronological Research, Nagoya University, Nagoya 464-8602, Japan,
[3]Graduate School of Environmental Sciences, Nagoya University, Nagoya 464-8602, Japan
[4]Institute of Regional Geological Survey of Jilin Province, Changchun 130022, China
[5]Institute of Geology and Geophysics, Chinese Academy of Sciences, Beijing 100029, China
(Received December 9, 2008 / Accepted December 28, 2008)

ABSTRACT

The Dongqing pluton in the Zhangguangcai Range, NE China comprises two-mica monzogranite and garnet-bearing two-mica monzogranite with subordinate garnet-bearing muscovite alkali-feldspar granite. The monzogranite was dated as 208 Ma by the $^{208}Pb/^{232}Th$ monazite dating (Fang, 1992) and ca. 160 Ma by the Rb-Sr and Sm-Nd methods (Wu *et al.*, 2004). To examine the discrepancy, monazite from the monzogranite was dated by the CHIME method coupled with age mapping. Monazite grains show significant compositional variation in concentric and sector fashions, but are chronologically uniform. Individual sets of ThO_2, UO_2 and PbO analyses were screened by the chemical criteria, $0.96<(Ca+Si)/(Th+U+Pb+S)<1.05$ and $K_2O<0.02$ wt.%. The screened data points are arrayed linearly on the PbO vs. ThO_2* diagram and define an isochron of 159.0±4.8 Ma with an intercept value of 0.0030±0.0017, suggesting that the older isotopic monazite age is possibly resulted from the sizable amounts of initial Pb. Present CHIME monazite dating reinforces that variety of peraluminous rocks in the Dongqing pluton formed at about 160 Ma through the late stage of magmatic differentiation and magma-fluid interaction.

INTRODUCTION

Voluminous granitoids were emplaced during the Paleozoic and Mesozoic eras in the Zhangguangcai Range that, together with Great and Lesser Xing'an Ranges, constitutes the eastern part of the Central Asian Orogenic Belt (Jahn *et al.*, 2001) in the northeastern part of China (Fig. 1). Although almost all of the granitoids in the Zhangguangcai Range are of I- and A-types (Wu *et al.*, 2000 and 2002) based on the criteria of Chappell and White (1974, 1992), only several plutons including the Dongqing pluton have been found to contain garnet and muscovite. Due to the presence of the peraluminous minerals, the plutons have been ascribed as the S-type

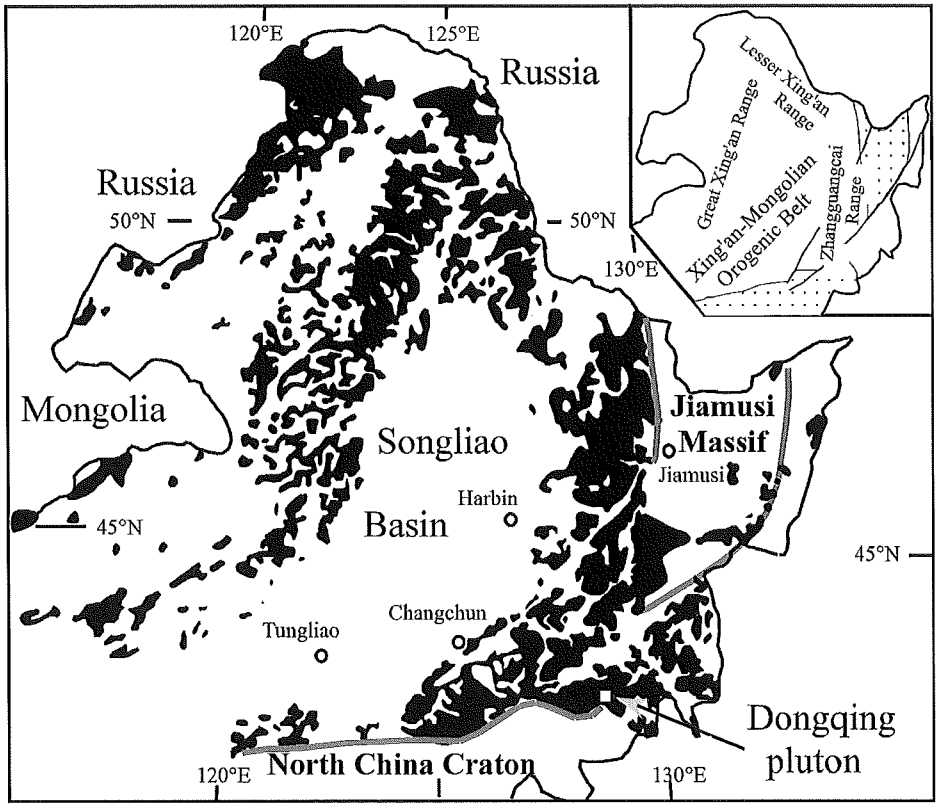

Fig. 1 Geological sketch map showing the widespread distribution of Phanerozoic granitoids in NE China (simplified from Jhan *et al.* (2001) and Wu *et al.* (2004)). Great Xing'an, Lesser Xing'an and Zhanguangcai are labeled in the upper-right inset.

granite and considered to be a product of collision between the Jiamusi Massif and the North China Craton (Fang, 1992; Peng and Su, 1997; Zhang, 1997). However, Jahn *et al.* (2001) suggested that some plutons with peraluminous minerals are of A- and I-types and can be formed by high degree of differentiation and intense fluid-magma interaction during the late stage of magmatic evolution.

The Dongqing pluton is situated in the south of the Zhangguangcai Range and comprises two-mica monzogranite and subordinate garnet-bearing muscovite alkali-feldspar granite (Fang, 1992; Wu *et al.*, 2004). Fang (1992) reported a monazite $^{208}Pb/^{232}Th$ age of 208 Ma for the two-mica monzogranite, and two muscovite K-Ar ages of 156 and 160 Ma for the granitic pegmatite in the Dongqing pluton, suggesting that two distinct emplacement stages should exist. Wu *et al.* (2004), on the other hand, concluded that the two types of granite were synchronously emplaced and underwent rapid cooling at about 160 Ma ago based on the Rb-Sr whole-rock isochron age and Rb-Sr and Sm-Nd whole-rock-mineral isochron ages. They also suggested that the peraluminous granites were highly fractionated I-type granite and that interaction between residual melt and aqueous hydrothermal fluid resulted in the REE patterns with large negative

Eu anomaly of garnet-bearing muscovite alkali-feldspar granites.

The chronological information is important to elucidate the genesis of the peraluminous Dongqing pluton, but the emplacement ages determined by Th-Pb and Rb-Sr whole-rock isochron methods are inconsistent. In this paper, we will present CHIME monazite age for garnet-bearing two-mica monzogranite of the Dongqing pluton and will discuss the cause of the inconsistency.

GEOLOGY AND SAMPLE DESCRIPTION

The Dongqing pluton is located about 60 km to the southwest of Antu, and composed mainly of two-mica monzogranite with subordinate garnet-bearing muscovite alkali-feldspar granite (Wu *et al.*, 2004). It has an exposed area of about 18 km^2 within the Dapuchaihe pluton composed of medium- to fine-grained biotite granodiorite with minor hornblende-bearing monzogranite and porphyritic monzogranite (Fig. 2).

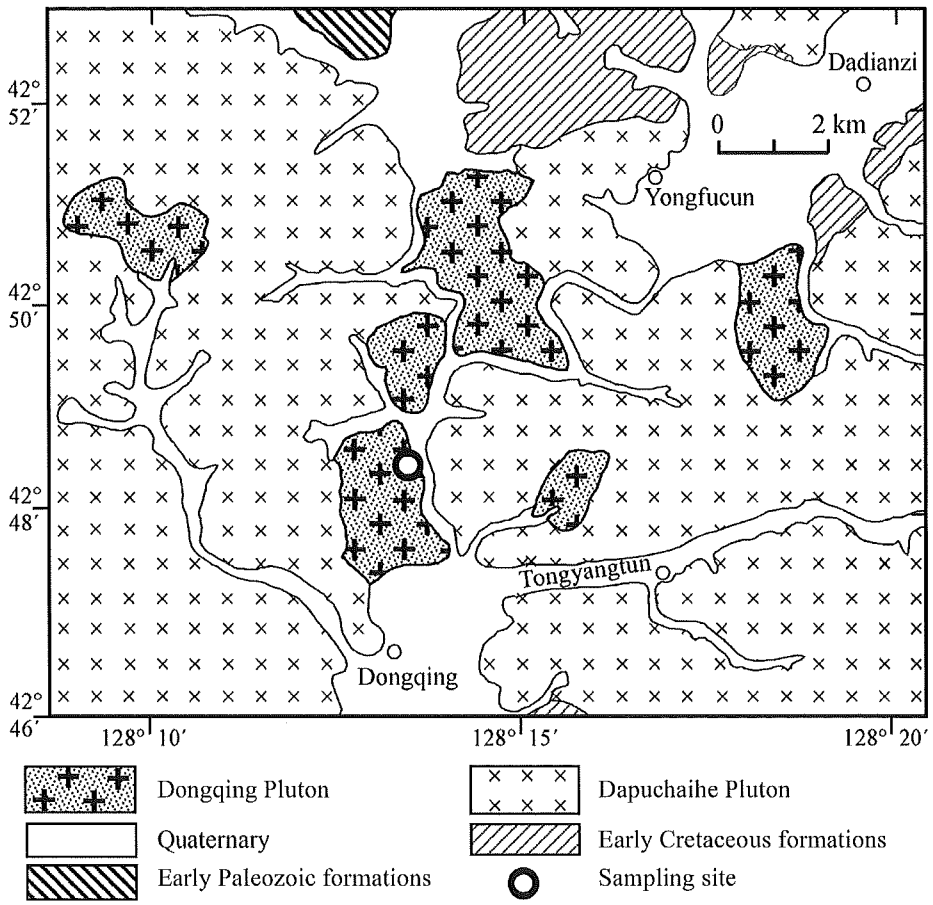

Fig. 2 The Dongqing pluton and the surrounding I type Dapuchaihe pluton (after Yin *et al.*, 1999). The solid circle shows our sampling site (42°48.519′N, 128°13.610′E).

The Dapuchaihe pluton is reported to have been formed during Cambrian period (Yin *et al.*, 1999), but a recent U-Pb zircon dating gives ages of 158–168 Ma (Zhang, unpublished data), very close to the formation time of Dongqing pluton. There is no clear direct contact relationship between Dongqing and Dapuchaihe plutons owing to sparse outcrops.

Samples were collected from an old quarry (42°48.519′N, 128°13.610′E). Rocks in the quarry are dominantly medium-grained garnet-bearing two-mica monzogranite with veins of garnet-bearing muscovite (±biotite) alkali-feldspar granite, aplite and pegmatite. Most veins are 5 to 10 cm in width, but large ones have a width over 50 cm.

Garnet-bearing two-mica monzogranite is composed of quartz (ca. 35 vol.%), microcline (ca. 30 vol.%), sodic oligoclase (ca. 25 vol.%), biotite (<5 vol.%), muscovite (<3 vol.%) and garnet (1–2 vol.%). Most plagioclase grains are normally zoned from An_{18}–An_{16} for the center to An_{10}–An_8 for the margin (Table 1). Garnet and biotite in garnet-bearing two-mica monzogranite show higher FeO and lower MgO contents than those reported by Wu *et al.* (2004), suggesting that the present sample is more evolved than two-mica monzogranite. Biotite contains 0.04–0.38 wt.% BaO with an average of 0.13 wt.% and microcline contains 0.01–0.41 wt.% BaO with an average of 0.19 wt.%.

Table 1. XRF analyses of garnet-bearing two-mica monzonite (1709a and 1709b) and garnet-bearing mucovite alkali-feldspar granite (1709c and 1709d) from the Dongqing pluton together with average compositions of two-mica monzonite (MG) and garnet-bearing mucovite alkali-feldspar granite (AfG) reported by Wu et al. (2004). Also listed are EPMA analyses of major constituent minerals in sample 1709a. Gt: garnet, Bt: biotite, Mus: muscovite, Kf: miclocline, Pl-core: plagioclase core, Pl-rim: plagioclase rim."*": total Fe as FeO.

	1709a	1709b	1709c	1709d	MG	AfG		Gt	Bt	Mus	Kf	Pl-core	Pl-rim
SiO_2	73.86	73.68	74.30	74.97	74.03	75.38	SiO_2	36.08	33.72	44.80	64.61	65.05	66.02
TiO_2	0.05	0.03	0.03	0.02	0.10	0.01	TiO_2	0.02	1.91	0.29	0.0	0.0	0.0
Al_2O_3	14.05	14.77	13.49	13.50	14.16	14.28	Al_2O_3	19.95	18.40	36.13	18.42	21.75	21.02
Fe_2O_3	–	–	–	–	0.06	0.90	Fe_2O_3	–	–	–	–	–	–
FeO	1.21*	1.25*	1.08*	0.90*	1.24	0.80	FeO	29.36*	27.31*	2.85*	0.02*	0.02*	0.01*
MnO	0.06	0.17	0.04	0.03	0.09	0.22	MnO	13.01	0.65	0.02	0.0	0.0	0.0
MgO	0.05	0.03	0.02	0.01	0.24	0.08	MgO	0.43	2.83	0.58	0.0	0.0	0.0
CaO	0.90	0.83	0.70	0.68	1.41	0.51	CaO	0.45	0.06	0.0	0.02	2.94	1.78
Na_2O	4.13	4.09	4.23	4.54	4.17	3.50	BaO	0.0	0.11	0.0	0.19	0.0	0.0
K_2O	4.01	3.96	4.26	4.27	3.69	4.41	Na_2O	0.0	0.03	0.0	0.80	9.83	10.51
P_2O_5	0.02	0.03	0.02	0.02	0.03	0.03	K_2O	0.0	8.89	10.55	15.59	0.24	0.23
LOI	0.30	0.37	0.17	0.12	0.58	0.49	LOI	–	–	–	–	–	–
Total	98.64	99.21	98.34	99.06	99.80	100.61	Total	99.30	93.91	95.22	99.65	99.83	99.57
V	3.3	4.1	3.6	4.3	–	–	Si	3.003	5.444	6.013	2.995	2.869	2.911
Cr	12	14	13	12	26.1	4.6	Ti	0.001	0.232	0.029	0.0	0.0	0.0
Co	1.1	1.5	1.0	1.0	–	–	Al	1.957	3.502	5.716	1.006	1.131	1.092
Ni	6.4	4.9	6.3	5.4	–	–	Fe	2.044	3.688	0.320	0.001	0.001	0.0
Zn	46	29	33	31	–	–	Mn	0.917	0.089	0.002	0.0	0.0	0.0
Rb	183	182	163	188	117	187	Mg	0.053	0.681	0.116	0.0	0.0	0.0
Sr	157	136	55	42	222	16	Ca	0.040	0.010	0.0	0.001	0.139	0.084
Y	22	27	19	15	7.82	36.8	Ba	0.0	0.007	0.0	0.003	0.0	0.0
Zr	55	48	20	5	75	32	Na	0.0	0.009	0.0	0.072	0.841	0.898
Ba	360	280	50	10	503	6.05	K	0.0	1.831	1.807	0.922	0.014	0.013
Pb	21	21	30	35	–	–	O =	12	22	22	8	8	8
Th	5.3	< 1.0	< 1.0	< 1.0	4.86	6.88							

Muscovite in garnet-bearing two-mica monzogranite contains no detectable amount of BaO. Alkali-feldspar granite shows higher modal quartz and microcline and lower modal plagioclase than garnet bearing two-mica monzogranite. Plagioclase is mainly albite in composition. Biotite, muscovite and garnet are sparse in the analyzed samples of alkali-feldspar granite. Monazite and zircon are rare in alkali-feldspar granite.

XRF analyses of garnet-bearing two-mica monzogranite (1709a and 1709b) and garnet-bearing alkali-feldspar granite (1709c and 1709d) are given in Table 1, together with average compositions of two-mica monzogranite and garnet-bearing muscovite alkali-feldspar granite reported by Wu *et al.* (2004). The bulk compositions of the garnet-bearing two-mica monzogranite are characterized by high contents of alkalis, with Na_2O = 4.13 wt.% and 4.09 wt.% and K_2O = 4.01 wt.% and 3.96 wt.%, respectively. Irrespective to presence of muscovite and garnet, the $Al_2O_3/(CaO+Na_2O+K_2O)$ molar ratios are 1.10 for sample 1709a and 1.18 for sample 1709b and the $Al_2O_3/(Na_2O+K_2O)$ molar ratios are 1.28 and 1.34, respectively. The $Al_2O_3/(CaO+Na_2O+K_2O)$ molar ratios of the garnet-bearing alkali-feldspar granites are 1.05 and 1.01, reflecting low modal abundance of biotite, muscovite and garnet. The concentrations of Ba, Sr and Zr in the garnet-bearing two-mica monzogranite are distinctly higher than those in the garnet-bearing alkali-feldspar granite, but not as high as in the two-mica monzogranite of Wu *et al.* (2004). Figure 3 compares primitive mantle-normalized spider diagrams of the garnet-bearing two-mica monzogranite (1709a) with those of averages of two-mica monzogranite and garnet-bearing muscovite alkali-feldspar granite of Wu *et al.* (2004). The normalized pattern of the two-mica monzogranite of Wu *et al.* (2004) shows high enrichment in Rb, Ba, Th and K and moderate enrichment of Sr, Zr and Y with negative anomalies of P and Ti. The normalized pattern of garnet-bearing

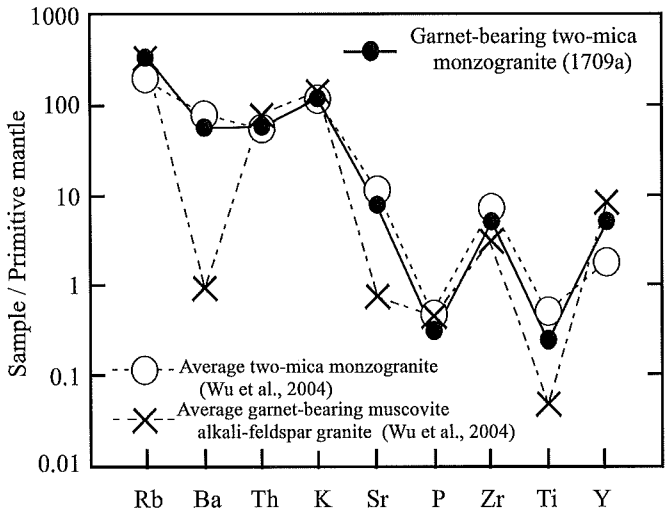

Fig. 3 Primitive mantle-normalized spider diagram for the garnet-bearing two-mica monzogranite (1709a). Normalization values from Sun and Mc Donough (1989). Also shown are primitive mantle-normalized spider diagrams for average two-mica monzogranite and garnet-bearing alkali-feldspar granite (Wu *et al.*, 2004).

muscovite alkali-feldspar granite shows significant depletion in Ba, Sr and Ti, while the Rb, Th and K concentrations remain unchanged. It is also depleted in Zr and enriched in Y.

The garnet-bearing two-mica monzogranite shows a normalized pattern similar to that of two-mica monzogranite. The intermediate characteristics of chemistry as shown by the slight depletion in Ba, Sr, Zr and Ti and the distinct enrichment in Y links the two-mica monzogranite and the garnet-bearing alkali-feldspar granite.

CHIME MONAZITE DATING

Experimental method

Monazite grains in polished thin sections were analyzed by using the JEOL JCXA-733 electron microprobe that was equipped with 4 wavelength dispersive spectrometers with a 140 mm radius of the Rowland circle. Each spectrometer was equipped with a PET (002 pentaerythritol) diffraction crystal and a sealed Xe X-ray detector.

Instrument operating conditions for the spot by spot analysis were 15 kV accelerating voltage, 3 μm probe diameter and 150 nA probe current. ThMα, UMβ, PbMα (PbMβ) and YLα lines were measured simultaneously, and CaKα, SKα, PKα, SiKα, KKα and NbLα lines were also measured. For the analyses of Th, U, Pb and Y, X-ray intensity was integrated over 400s period for the line peak position and over 200s period for two optimum background positions. To ensure that possible changes of the sample surface had a minimal effect on the results, the measurement of peak and background positions was repeated five times for each analysis. For the analyses of other elements, X-ray intensities were integrated over 40s on each line peak position and 20s on two background positions. The background value for each line was estimated by exponential fitting of two readings. The standards were euxenite provided by Smellie *et al.* (1978) for Th, U and Nb, synthesized glass (Suzuki and Adachi, 1998) for Pb, Si and Ca, synthesized Y-glass (Y_2O_3 = 10 wt.% and K_2O = 2 wt.%) for Y and K, barite for S, xenotime for P and the synthesized REE glasses provided Drake and Weill (1972) for rare earth elements. The interferences of ThMγ, ThM3–N4 and ThM5–P3 lines on UMβ and NbLβ, YLγ, ThMζ and SKα lines on PbMα were corrected through the procedures described in Suzuki and Kato (2008). The X-ray intensity data were converted into concentrations by the Bence and Albee's method (Bence and Albee, 1968) using the a-factor table provided by Kato (2005) and the average of analyses on several spots as the matrix composition. The small difference in the matrix compositions between analyzed and reference spots has a negligible effect on the ThO_2, UO_2 and PbO determinations. The detection limits at a 2σ confidence level were 0.009, 0.011 and 0.006 wt.% for ThO_2, UO_2 and PbO, respectively. Relative errors were about 10% for 0.03 wt.% PbO, 5% for 0.07 wt.% PbO, 2% for 0.6 wt.% UO_2 and 0.5% for 7.0 wt.% ThO_2. The CHIME age was calculated through the procedure given in Suzuki and Adachi (1991a and 1991b) and Suzuki and Kato (2008, and references therein) by using the decay constants recommended by Steiger and Jäger (1977).

For digital mapping of monazite, we used 3 spectrometers for the Pb measurement with a beam current of 600 nA. The rest spectrometer is used for acquiring a background map. Background maps for individual line positions of every spectrometer

were calculated through the intensity relationships determined in advance of the measurement. The ThMα, UMβ and YLγ intensities were measured prior to the PbMα and background acquisitions with a probe current of 210 nA. The pixel step was 4 μm and the dwell time per pixel was 5s for the acquisition of PbMα and background and 3s for the acquisition of ThMα, UMβ and YLγ. We further shortened the measurement time by skipping the area outside monazite. The high probe current sometimes causes severe damage on monazite surface and carbon coating at and around metamict portions, cleavages and cracks, which is evident by comparison BSE images in Figs. 4 and 5 with those in Fig. 6. This damage renders the surface of the grain unsuitable for precise determination of the Th, U and Pb contents. We, therefore, carried out the spot by spot analysis before the digital mapping

Age mapping

Most monazite grains in two-mica monzogranite are low in Th and U. Figure 4 shows the result of digital mapping of M01 (upper) and M03 (lower) monazite grains located at the boundary between plagioclase and quartz. The backscattered electron image shows a significant heterogeneity within grains. The ThO_2 concentration ranges from 4 to 13 wt.% and is mostly below 7 wt.%. It is high in the central and marginal domains separated by troughs. Within a single zone, different sectors show different

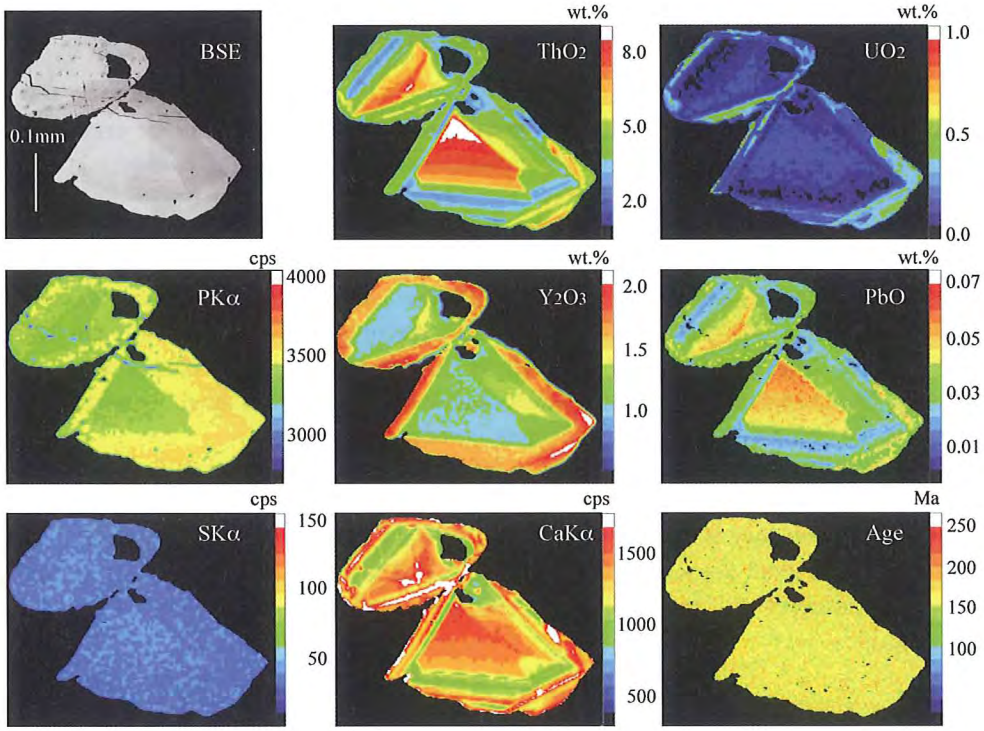

Fig. 4 Back scattered electron (BSE) image, compositional maps and a chronological map of M01 (upper) and M03 (lower) monazite grains in 1709a garnet-bearing two-mica monzogranite.

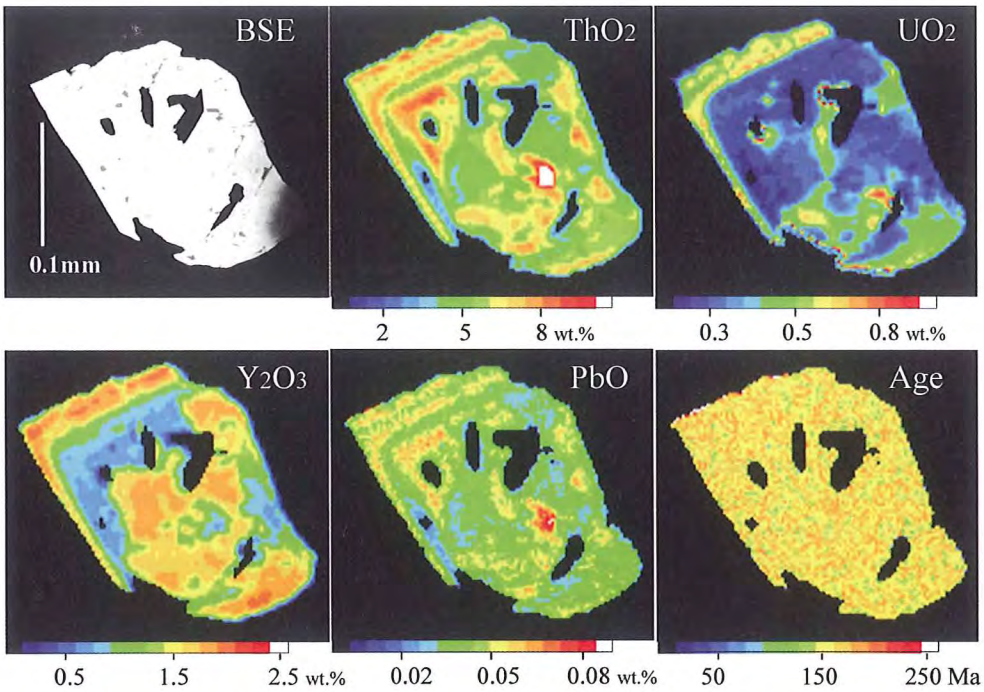

Fig. 5 Back scattered electron (BSE) image, compositional maps and a chronological map of M02 monazite grain in 1709a garnet-bearing two-mica monzogranite.

concentrations. Such concentric and sector zoning might be formed by crystallization from viscous magma. The UO_2 concentration, 0.1 to 0.7 wt.%, is approximately covariant with the ThO_2 concentration. The CaKα counts, being corresponding to 0.4 to 1.2 wt.% CaO, are covariant with the ThO_2 and UO_2 concentrations. The SKα intensities within the monazite grains are of the background level, suggesting a significant amount of bravandite substitution with a negligible amount of the $CaSO_4$ substitution (Suzuki and Kato, 2008) in monazite. The Y_2O_3 distribution is reverse with the ThO_2 distributions. The apparent ages are uniform throughout grains and cluster at around 160 Ma. This together with the compositional zoning suggests a single generation of monazite by crystallization from a viscous granitic melt.

Figure 5 shows the digital mapping of M02 monazite grain in contact with biotite, muscovite and microcline. This grain shows irregular distribution of Th and U in the center and oscillatory zoning in the margin. The Y_2O_3 concentration is high in the central and marginal domains. This grain, like M01 grain, is chronologically uniform with apparent ages of around 160 Ma, suggesting no inherited older component within the grain.

CHIME monazite age

A total of 114 spots were analyzed on M01, M02 and M03 grains to calculate the CHIME age (Fig. 6). The analytical results are listed in Table 2. The S concentration is below the detection limits (0.003 wt.%) for most spots, but spots M01-24, M01-25,

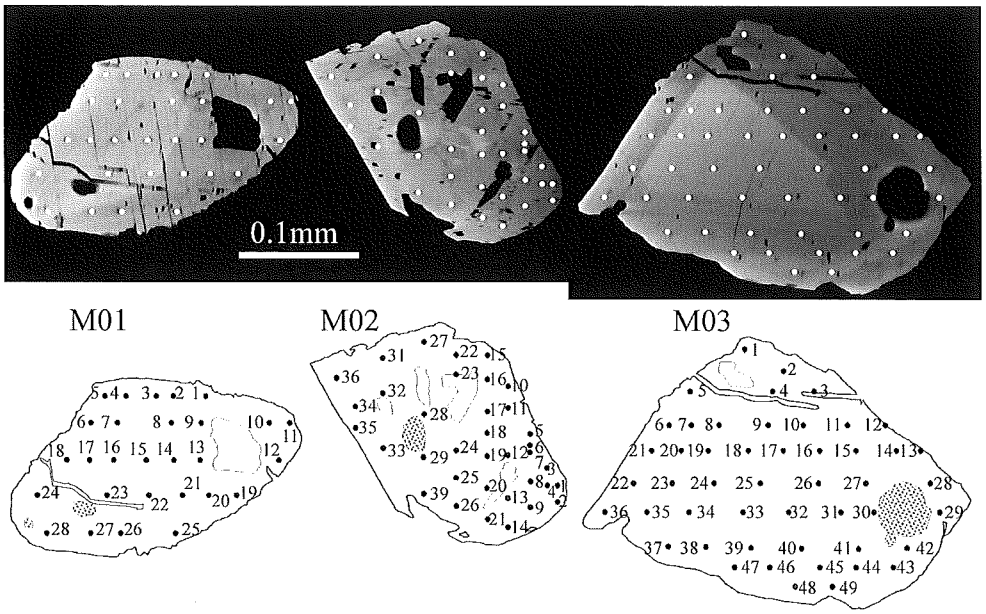

Fig. 6 Back scattered electron (BSE) images of M01, M02 and M03 monazite grains after the digital mapping, showing analyzed spots. The numbers given to individual spots correspond to the spot numbers given in Table 2. The dotted areas in sketch maps represent portions where included minerals appear by additional polishing of the thin section after the digital mapping (compare BSE images in Figs. 4 and 5). Gaps developed along cleavages in M01 grain.

Table 2. Electron microprobe analyses (wt.%) of monazite in 1907a garnet-bearing two-mica monzogranite. Age: apparent age in Ma, ThO_2*: the measured ThO_2 plus ThO_2 equivalent of the measured UO_2, R: the molar $(CaO+SiO_2)/(ThO_2+UO_2+PbO+S)$ ratio.

Spot	ThO_2	UO_2	PbO	Age	ThO_2*	CaO	Y_2O_5	S	K_2O	SiO_2	R
M01-01	5.36	0.463	0.0441	152	6.85	0.953	1.755	<0.002	0.017	0.354	1.03
M01-02	5.92	0.308	0.0505	173	6.91	0.897	1.327	<0.002	0.018	0.479	1.01
M01-03	7.20	0.606	0.0654	169	9.15	1.195	1.494	<0.002	0.017	0.511	1.00
M01-04	5.02	0.227	0.0423	174	5.75	0.810	1.808	<0.002	0.018	0.339	1.00
M01-05	7.08	0.716	0.0615	155	9.38	1.251	1.931	<0.002	0.027	0.420	0.99
M01-06	7.56	0.545	0.0643	163	9.32	1.092	2.101	<0.002	0.011	0.684	1.00
M01-07	6.95	0.543	0.0602	164	8.70	1.207	1.862	<0.002	0.006	0.407	0.99
M01-08	6.16	0.164	0.0524	185	6.69	0.728	1.046	<0.002	0.013	0.644	0.98
M01-09	9.98	0.211	0.0750	166	10.66	1.153	0.931	<0.002	0.008	1.145	1.02
M01-10	4.85	0.130	0.0384	172	5.27	0.643	1.141	<0.002	0.003	0.465	1.01
M01-11	6.59	0.374	0.0508	154	7.79	1.136	1.774	<0.002	0.015	0.355	0.98
M01-12	7.19	0.549	0.0603	159	8.96	1.140	1.981	<0.002	0.011	0.540	0.99
M01-13	7.58	0.187	0.0491	142	8.18	0.886	1.095	<0.002	0.011	0.718	0.94
M01-14	10.94	0.226	0.0813	165	11.67	1.192	1.145	<0.002	0.005	1.272	0.99
M01-15	9.53	0.197	0.0698	162	10.16	1.026	0.868	<0.002	0.009	1.141	1.00
M01-16	6.55	0.131	0.0487	165	6.97	0.719	0.783	<0.002	0.011	0.765	1.00
M01-17	5.37	0.113	0.0409	169	5.73	0.703	0.894	<0.002	<0.004	0.503	1.00
M01-18	4.73	0.163	0.0379	171	5.26	0.721	1.758	<0.002	<0.004	0.295	0.95
M01-19	6.08	0.326	0.0492	163	7.13	0.991	1.647	<0.002	0.009	0.407	1.00
M01-20	6.90	0.188	0.0521	164	7.50	0.873	1.222	<0.002	0.009	0.690	1.00

Table 2. (continued)

Spot	ThO_2	UO_2	PbO	Age	ThO_2*	CaO	Y_2O_5	S	K_2O	SiO_2	R
M01-21	9.34	0.222	0.0717	169	10.06	1.156	1.404	<0.002	0.006	0.946	1.00
M01-22	12.67	0.236	0.1022	180	13.44	1.179	0.890	<0.002	0.004	1.481	0.93
M01-23	10.20	0.207	0.0762	166	10.87	1.045	0.875	<0.002	0.008	1.278	1.00
M01-24	5.28	0.206	0.0434	173	5.94	0.831	1.923	0.005	0.003	0.394	1.01
M01-25	7.12	0.584	0.0611	161	9.00	1.196	2.042	0.005	0.008	0.511	1.01
M01-26	5.93	0.232	0.0496	176	6.68	0.867	1.532	<0.002	0.003	0.489	1.00
M01-27	8.47	0.217	0.0637	164	9.17	1.052	1.192	<0.002	0.014	0.832	0.98
M01-28	7.25	0.360	0.0596	168	8.41	0.993	1.257	<0.002	0.013	0.664	0.99
M02-01	5.90	0.418	0.0544	177	7.25	0.893	1.692	0.011	0.019	0.559	1.03
M02-02	5.94	0.501	0.0568	178	7.56	0.921	1.904	0.012	0.032	0.557	1.03
M02-03	5.52	0.273	0.0464	172	6.40	0.764	1.313	0.005	0.009	0.546	1.02
M02-04	5.81	0.385	0.0499	167	7.05	0.840	1.554	0.010	0.012	0.541	1.00
M02-05	5.28	0.104	0.0455	192	5.62	0.567	0.782	0.008	0.009	0.597	0.96
M02-06	5.28	0.104	0.0429	181	5.62	0.567	0.782	0.008	0.009	0.628	0.99
M02-07	7.57	0.225	0.0611	174	8.29	0.949	1.101	<0.002	0.011	0.817	1.02
M02-08	5.12	0.401	0.0550	203	6.42	0.882	1.675	<0.002	0.014	0.511	1.15
M02-09	6.02	0.496	0.0550	171	7.62	0.918	1.987	<0.002	0.009	0.519	1.01
M02-10	6.71	0.411	0.0539	159	8.03	0.968	1.501	0.002	0.008	0.550	0.97
M02-11	6.86	0.163	0.0499	160	7.38	0.785	1.188	0.002	0.004	1.021	1.15
M02-12	5.44	0.299	0.0466	172	6.40	0.963	1.861	0.003	0.008	0.316	1.02
M02-13	4.84	0.447	0.0401	151	6.27	0.975	1.534	0.010	0.011	2.762	3.10
M02-14	6.39	0.554	0.0561	162	8.18	1.053	2.020	<0.002	0.011	0.501	1.02
M02-15	4.80	0.184	0.0306	134	5.39	0.829	1.964	<0.002	0.010	0.368	1.10
M02-16	5.98	0.373	0.0553	182	7.18	0.899	1.716	<0.002	0.006	0.521	1.02
M02-17	4.81	0.162	0.0367	163	5.33	0.766	1.918	<0.002	0.008	0.321	1.00
M02-18	4.95	0.178	0.0398	170	5.53	0.771	1.755	0.003	0.006	0.397	1.03
M02-19	11.26	0.284	0.0869	169	12.18	0.983	0.830	0.002	0.012	1.623	1.01
M02-20	7.54	0.671	0.0673	164	9.70	1.394	1.940	<0.002	0.009	0.398	1.00
M02-21	4.42	0.228	0.0394	181	5.16	0.707	1.354	<0.002	0.016	0.996	1.64
M02-22	3.80	0.088	0.0295	171	4.08	0.492	1.013	<0.002	0.005	0.358	0.99
M02-23	1.77	2.123	0.0186	51	8.56	0.126	0.182	0.002	2.875	35.938	40.78
M02-24	5.06	0.159	0.0408	173	5.57	0.679	1.343	<0.002	0.007	0.471	1.00
M02-25	5.35	0.275	0.0529	200	6.24	0.936	1.721	<0.002	0.007	0.561	1.21
M02-26	6.51	0.448	0.0584	174	7.96	0.945	1.699	0.005	0.022	0.560	0.98
M02-27	5.80	0.310	0.0425	148	6.80	0.989	1.310	0.003	0.009	2.930	2.84
M02-28	5.46	0.231	0.0436	166	6.20	0.890	1.922	<0.002	<0.004	0.327	0.98
M02-29	4.83	0.184	0.0394	172	5.42	0.785	1.981	<0.002	0.006	0.316	1.01
M02-30	5.71	0.371	0.0489	167	6.91	0.778	1.662	<0.002	0.029	0.540	0.98
M02-31	6.92	0.522	0.0615	169	8.60	1.178	1.624	<0.002	0.014	0.431	0.99
M02-32	6.42	0.100	0.0505	177	6.74	0.694	0.796	<0.002	0.007	0.746	1.00
M02-33	2.76	0.087	0.0173	134	3.05	0.403	0.680	<0.002	0.023	1.596	3.10
M02-34	5.92	0.129	0.0446	167	6.33	0.663	0.942	0.002	0.004	0.661	0.98
M02-35	7.49	0.735	0.0688	165	9.85	1.344	1.843	<0.002	0.013	0.494	1.03
M02-36	7.05	0.547	0.0618	166	8.82	1.078	1.850	0.002	0.010	0.573	0.99
M03-01	3.77	0.100	0.0313	181	4.10	0.493	0.958	<0.002	0.005	0.356	0.99
M03-02	5.57	0.146	0.0420	164	6.04	0.766	1.201	<0.002	<0.004	0.465	0.98
M03-03	6.08	0.363	0.0588	192	7.25	1.080	1.604	<0.002	0.031	1.668	1.91
M03-04	6.30	0.131	0.0460	162	6.72	0.774	1.000	<0.002	<0.004	0.682	1.02
M03-05	5.04	0.135	0.0392	169	5.47	0.716	1.416	<0.002	<0.004	0.398	0.98
M03-06	5.61	0.259	0.0443	163	6.45	0.851	1.657	0.003	0.012	0.459	1.01
M03-07	12.98	0.234	0.0938	161	13.74	1.244	0.930	<0.002	0.011	1.614	0.97
M03-08	12.92	0.221	0.0892	155	13.64	1.218	0.921	<0.002	0.016	1.672	0.99
M03-09	8.28	0.194	0.0660	175	8.91	1.102	1.352	<0.002	0.009	0.813	1.02
M03-10	7.67	0.204	0.0583	166	8.32	1.063	1.364	<0.002	0.005	0.656	0.99
M03-11	6.10	0.425	0.0517	164	7.47	1.021	1.901	<0.002	0.007	0.428	1.02

Table 2. (continued)

Spot	ThO_2	UO_2	PbO	Age	ThO_2*	CaO	Y_2O_5	S	K_2O	SiO_2	R
M03-12	3.60	2.650	0.0244	48	12.06	0.641	0.707	0.006	6.004	21.998	15.90
M03-13	5.97	1.255	0.0518	122	10.00	0.752	1.669	<0.002	2.294	9.331	6.13
M03-14	9.36	0.814	0.0847	167	11.98	1.513	2.329	<0.002	0.013	0.719	1.00
M03-15	5.86	0.162	0.0468	173	6.39	0.798	1.385	<0.002	0.004	0.549	1.02
M03-16	7.94	0.212	0.0592	162	8.62	1.119	1.528	<0.002	0.006	0.668	1.00
M03-17	10.68	0.214	0.0766	159	11.37	1.177	1.148	<0.002	0.004	1.169	0.97
M03-18	12.16	0.215	0.0913	168	12.85	1.174	0.967	<0.002	0.010	1.351	0.92
M03-19	11.87	0.207	0.0837	158	12.54	1.169	0.977	0.004	0.006	1.468	0.98
M03-20	11.95	0.218	0.0927	173	12.65	1.174	0.968	<0.002	0.008	1.525	1.00
M03-21	5.43	0.149	0.0413	165	5.91	0.768	1.548	<0.002	0.006	0.442	0.99
M03-22	5.38	0.137	0.0462	188	5.82	0.738	1.476	<0.002	0.008	0.463	0.99
M03-23	10.81	0.199	0.0801	165	11.46	1.091	0.937	<0.002	0.011	1.327	0.99
M03-24	10.89	0.203	0.0807	165	11.54	1.081	0.961	<0.002	0.009	1.369	0.99
M03-25	11.07	0.193	0.0833	168	11.69	1.114	0.966	<0.002	0.008	1.380	1.00
M03-26	11.04	0.214	0.0815	164	11.73	1.148	1.040	<0.002	0.011	1.365	1.00
M03-27	7.38	0.223	0.0584	171	8.10	1.050	1.577	<0.002	0.006	0.621	1.00
M03-28	9.44	0.627	0.0796	164	11.46	1.273	2.453	0.003	0.018	0.983	1.01
M03-29	5.29	0.457	0.0455	159	6.77	0.823	2.099	<0.002	0.012	0.449	1.01
M03-30	4.96	0.088	0.0385	174	5.24	0.685	1.176	<0.002	0.004	0.417	0.99
M03-31	6.26	0.130	0.0432	153	6.68	0.816	1.215	<0.002	<0.004	0.576	0.99
M03-32	9.77	0.167	0.0726	167	10.31	1.021	0.931	<0.002	0.012	1.184	1.00
M03-33	9.62	0.165	0.0679	158	10.15	1.001	0.962	<0.002	0.006	1.151	0.99
M03-34	8.05	0.141	0.0643	179	8.50	0.849	0.883	<0.002	0.008	0.962	1.00
M03-35	7.55	0.112	0.0579	173	7.91	0.867	0.885	<0.002	0.004	0.870	1.02
M03-36	6.21	0.426	0.0484	151	7.58	1.042	1.924	<0.002	0.008	0.388	0.99
M03-37	6.00	0.270	0.0482	166	6.87	1.037	1.897	<0.002	0.007	0.324	1.00
M03-38	4.82	0.152	0.0361	161	5.31	0.777	1.827	<0.002	0.011	0.308	1.00
M03-39	4.72	0.113	0.0363	169	5.08	0.720	1.896	<0.002	0.009	0.325	0.99
M03-40	4.46	0.103	0.0324	160	4.79	0.673	1.739	<0.002	0.004	0.308	0.98
M03-41	5.86	0.377	0.0516	173	7.07	0.832	1.739	<0.002	0.007	0.548	1.01
M03-42	7.55	0.582	0.0664	167	9.42	0.977	2.626	<0.002	0.014	0.820	1.00
M03-43	8.60	0.621	0.0716	160	10.60	1.119	2.259	0.003	0.009	0.857	0.97
M03-44	7.86	0.504	0.0702	175	9.49	0.910	2.224	0.003	0.005	0.990	1.02
M03-45	6.28	0.354	0.0504	161	7.42	1.097	1.757	<0.002	0.009	0.713	1.24
M03-46	6.91	0.339	0.0584	173	8.01	1.169	1.820	<0.002	0.008	0.436	1.01
M03-47	6.90	0.417	0.0578	166	8.24	1.173	1.837	<0.002	0.005	0.445	1.01
M03-48	4.96	0.438	0.0463	172	6.37	0.789	1.959	0.002	<0.004	0.407	1.01
M03-49	7.94	0.456	0.0660	166	9.41	0.924	2.059	<0.002	0.012	0.933	1.00
M03-50	8.85	0.564	0.0784	178	10.67	1.084	2.052	<0.002	0.012	0.936	0.97

M02-01, M02-02, M02-04, M02-13 and M03-12 contain 0.005–0.012 wt.% S. Some data sets (M02-23, M03-12, and M03-13 in Table 2) show extremely high SiO_2 and K_2O contents. These analyses were resulted from hitting on grain margins or around inclusions of biotite or K-feldspar. Similarly, the high SiO_2 analyses (M02-27 and M02-32) were resulted from hitting around quartz inclusions. Spots M01-13 and M02-08 locate on metamict domains where the (Ca+Si)/(Th+U+Pb+S) ratio deviates largely from unity. Therefore, the apparent ages of 203 Ma for M02-27 and 142 Ma for M01-13 are likely discordant. To regress an isochron free from potentially discordant data points, individual analyses were screened with the chemical criteria, $0.95<(Ca+Si)/(Th+U+Pb+S)<1.05$ and $K_2O<0.02$ wt.% (Suzuki and Kato, 2008). The screened 89 data

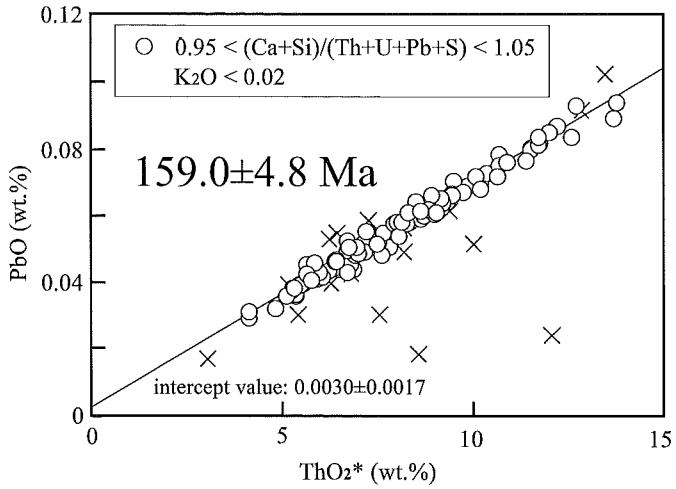

Fig. 7 PbO vs. ThO_2* plots of M01, M02 and M03 monazite grains. ThO_2* denotes sum of the measured ThO_2 and ThO_2 equivalent to the measured UO_2. Circles represent data points screened with the chemical criteria, $0.95<(Ca+Si)/(Th+U+Pb+S)<1.05$ and $K_2O<0.02$ wt.%, and crosses show data points rejected by the criteria.

points are arrayed linearly and give an isochron of 159.0±4.8 Ma with an intercept value of 0.0030±0.0017 (Fig. 7).

DISCUSSION

Emplacement time of the Dongqing pluton

Previous $^{208}Pb/^{232}Th$ monazite dating gave a 208 Ma age for the two-mica monzogranite in the Dongqing pluton, and K-Ar dating of mica gave 156 and 160 Ma ages for the granitic pegmatites (Fang, 1992). On the basis of the age difference, Fang (1992) suggested two different stages for the pluton emplacement. Recent Rb-Sr isotopic study gave a whole-rock isochron age of 156±3 Ma based on the 4 isotopic analyses of two-mica monzogranite and an isotopic analysis of garnet-bearing alkali-feldspar granite (Wu *et al.*, 2004). They also reported 158±2 Ma Rb-Sr mineral isochron ages for of two-mica monzogranite and 153±3 Ma Rb-Sr and 162±4 Ma Sm-Nd mineral isochron ages for garnet-bearing alkali-feldspar granite. Wu *et al.* (2004) considered that both two-mica monzogranite and garnet-bearing alkali-feldspar granite emplaced at about 160 Ma, but did not interpret the cause of the inconsistency between $^{208}Pb/^{232}Th$ monazite and Rb-Sr isochron ages.

Present digital mapping reveals that monazite grains in garnet-bearing two-mica monzogranite show oscillatory and sector zonings typical for growth from viscous magma, but are chronologically homogeneous with ca. 160 Ma apparent ages (Figs. 4 and 5). Monazite grains do not contain older components leading the $^{208}Pb/^{232}Th$ age of 208 Ma. The refined CHIME monazite age is 159.0±4.8 Ma, consistent with the Rb-Sr and Sm-Nd ages reported by Wu *et al.* (2004). Before we adopt our CHIME monazite age, it is of interest to discuss how the 208 Ma $^{208}Pb/^{232}Th$ monazite age was

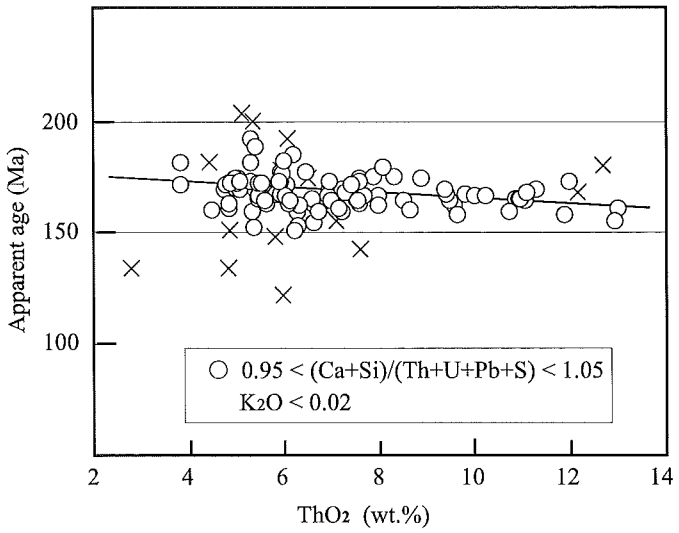

Fig. 8 Plots of apparent age against the ThO_2 concentration of monazite. Symbols are the same as in Fig. 6.

generated. As stated above, the intercept value of isochron is 0.0030±0.0017. Although it is close to zero within the limit of analytical uncertainty, the positive value suggests sizable amounts of initial Pb in monazite. To confirm this, the relationship between the ThO_2 concentration and apparent ages is illustrated in Fig. 8. Datasets with lower ThO_2 concentrations tend to give higher apparent ages than those with higher ThO_2 concentrations, reinforcing sizable amounts of common Pb in monazite. If monazite grains analyzed by Fang (1992) were low in ThO_2 and high in initial Pb, erroneous old $^{208}Pb/^{232}Th$ age might be possible without appropriate common Pb correction. Further, datasets with the (Ca+Si)/(Th+U+Pb+S) ratio deviated from unity give apparent ages over 200 Ma (e.g. M02-08, N02-25 and M03-03) as well as younger ages (e.g. M01-13 and M02-15). The $^{208}Pb/^{232}Th$ age of 208 Ma appears to be discordant owing to the common Pb effect and the non-closed system behavior of the Th-Pb system. The present CHIME monazite age of 159.0±4.8 Ma appears to be the crystallization time of the garnet-bearing two-mica monzogranite. This dating and the Rb-Sr and Sm-Nd isochron ages of Wu *et al.* (2004) strongly suggest that the ca. 160 Ma age most likely dates the emplacement age of the Dongqing pluton.

Mineralogy during the late stage of magma-fluid interaction

Wu *et al.* (2004) considered that the garnet-bearing alkali-feldspar granite was formed contemporaneously with two-mica monzogranite by intense magma-fluid interaction during the late stage of differentiation of A- or I-type magmas. The present CHIME dating and previous isotopic dating (Fang, 1992; Wu *et al.*, 2004) confirm the simultaneity of the monzogranite and alkali-feldspar granite. The change from the two-mica monzogranite to the garnet-bearing alkali-feldspar granite may be realized through formation of garnet at the expense of biotite and plagioclase:

$$\underset{\text{biotite}}{K_2Fe_6Al_2Si_6O_{20}(OH)_4} + \underset{\text{plagioclase}}{CaAl_2Si_2O_8 + 2NaAlSi_3O_8} + 4H^+$$

$$\rightarrow \underset{\text{garnet}}{2Fe_3Al_2Si_3O_{12}} + \underset{\text{K-feldspar}}{2KAlSi_3O_8} + \underset{\text{quartz}}{2SiO_2} + Ca^{2+} + 2Na^+ + 4H_2O$$

Barium and Ti in biotite (see Table 1) and Sr in plagioclase were released into fluid during this reaction and garnet likely incorporates Y from fluid by $Y^{3+}Al^{3+} \rightleftarrows Mn^{2+}Si^{4+}$ (Jaffe, 1951) and $Y^{3+} \rightleftarrows Al^{3+}$ (Wang *et al.*, 2003) substitutions. This process resulted in significant depletion in Ba, Sr, and Ti and enrichment in Y in the garnet-bearing alkali-feldspar granite. The persistence of Ba-bearing biotite and oligoclase in the garnet-bearing two-mica monzogranite is consistent with its intermediate characteristics in terms of Ba, Sr, Ti and Y concentrations (Fig. 3). Mineral species provide constraint on element abundances in rocks formed through intense magma-fluid interaction.

CONCLUSIONS

(1) The Dongqing pluton in the Zhangguangcai Range includes two-mica monzogranite, garnet-bearing alkali-feldspar granite and garnet-bearing two-mica monzogranite

(2) Digital mapping reveals that monazite grains in garnet-bearing two-mica monzogranite display concentric and sector zoning, but they are chronologically uniform throughout grains. Spot by spot analyses are filtered by the chemical criteria, $0.95<(Ca+Si)/(Th+U+Pb+S)<1.05$ and $K_2O<0.020$ wt.%. The screened datasets define an isochron of 159.0±4.8 Ma with an intercept value of 0.0030±0.0017. This age is younger than the $^{208}Pb/^{232}Th$ monazite age of 208 Ma (Fang, 1992), but accords well with Rb–Sr and Sm–Nd isochron ages reported by Wu *et al.* (2004). The older $^{208}Pb/^{232}Th$ monazite age is most likely caused by the sizable amounts of initial Pb in monazite.

(3) The development of garnet-bearing alkali-feldspar granite in the Dongqin pluton is ascribable to the formation of garnet through decomposition of biotite and plagioclase as the result of intense fluid-magma interaction during a late stage of magmatic evolution.

ACKNOWLEGEMENTS

We thank Professors Wenliang Xu, Jian Wang and Iwao Kawabe for the constructive review of the manuscript. Drs. Changqing Zheng and Takenori Kato are acknowledged for fruitful discussions. This research was partially supported by the Ministry of Education, Science, Sports and Culture, Grant-in-Aid for Scientific Research (B), No. 19340149, 2008.

REFERENCES

Bence, A.E., Albee, A.L. (1968): Empirical correction factors for the electron microanalysis of silicates and oxides. *Journal of Geology*, **76**, 382–403.

Chappell, B.W., White, A.J.R. (1974): Two contrasting granite types. *Pacific Geology*, No.8,

173–174.
Chappell, B.W., White, A.J.R. (1992): I- and S-type granites in the Lachlan Fold Belt. Transactions of Royal Society of Edinburgh: *Earth Sciences*, **83**, 1–26.
Fang, W.-C. (1992): The granitoids and their mineralizations in Jilin Province, Jilin Publishing House of Science and Technology, Changchun, p. 271 (in Chinese).
Drake, M.J., Weill, D.F. (1972): New rare earth element standards for electron microprobe analysis. *Chemical Geology*, **10**, 179–181.
Jaffe, H.W. (1951): The role of yttrium and other minor elements in the garnet group. *American Mineralogist*, **36**, 133–155.
Jahn, B.-M., Wu, F.-Y., Capdevila, R., Fourcade, S., Wang, Y.-X., Zhao, Z.-H. (2001): Highly evolved juvenile granites with tetrad REE patterns: the Woduhe and Baerzhe granites from the Great Xing'an (Khingan) Mountains in NE China. *Lithos*, **59**, 171–198.
Kato, T. (2005): New accurate Bence-Albee a-factors for oxides and silicates calculated from the PAP correction procedure. *Geostandards and Geoanalytical Research*, **29**, 83–94.
Peng, Y.-J., Su, Y.-Z. (1997): Geotectonic characteristics of central Jilin Province. *Memoirs of Shenyang Institute of Geology and Mineral Resources, Chinese Academy of Geological Sciences* (5–6), 335–376. (in Chinese with English abstract).
Smellie, J.A.T., Cogger, N., Herrington, J. (1978): Standards for quantitative microprobe determination of uranium and thorium with additional information on the chemical formulae of davidite and euxenite-polycrase. *Chemical Geology*, **22**, 1–10.
Steiger, R.H., Jäger, E. (1977): Subcommission on geochronology: convention on the use of decay constants in geo- and cosmochronology. *Earth and Planetary Science Letters*, **36**, 359–362.
Sun, S.S., Mc Donough, W.F. (1989): Chemical and isotopic systematics of oceanic basalts: implications for mantle composition and processes. In Saunders, A.D., Norry, M.J. (Eds) Magmatism in Ocean Basins. *Geological Society of London Special Publication*, No.43, 313–345.
Suzuki. K., Adachi, M. (1991a): Precambrian provenance and Silurian metamorphism of the Tsubonosawa paragneiss in the South Kitakami terrane, Northeast Japan, revealed by the chemical Th-U-total Pb isochron ages of monazite, zircon and xenotime. *Geochemical Journal*, **25**, 357–376.
Suzuki. K., Adachi, M. (1991b): The Chemical Th-U-total Pb Isochron Ages of Zircon and Monazite from the Gray Granite of the Hida Terrane, Japan. *The Journal of Earth and Planetary Sciences, Nagoya University*, **38**, 11- 38.
Suzuki, K., Adachi, M. (1998): Denudation history of the high T/P Ryoke metamorphic belt, Southwest Japan: constraints from CHIME monazite ages of gneisses and granitoids. *Journal of Metamorphic Geology*, **16**, 23–37.
Suzuki, K. and Kato, T. (2008): CHIME dating of monazite, xenotime, zircon and polycrase: protocol, pitfalls and chemical criterion of possibly discordant age data. *Gondwana Research*, **14**, 569–586.
Wang, R.-C., Hu, H.-A., Zhang, A.-C., Xu, S.-J. and Wang. D.-Z. (2003): Yttrium zoning in garnet from the Xihuashan granite complex and its petrological implications. *Chinese Science Bulletin*, **48**, 1611–1615.
Wu, F.-Y., Jahn, B.-M., Wilde, S.A., Sun, D.-Y. (2000): Phanerozoic crustal growth: U–Pb and Sr–Nd isotopic evidence from the granites in northeastern China. Tectonophysics, **328**, 89–113.
Wu, F.-Y., Sun, D.-Y., Li, H.-M., Jahn, B.-M., Wilde, S.A. (2002): A-type granites in Northeastern China: age and geochemical constraints on their petrogenesis. *Chemical Geology*, **187**, 143–173.
Wu, F.-Y., Sun, D.-Y., Jahn, B.-M. and Wilde, S. (2004): A Jurassic garnet-bearing granitic pluton from NE China showing tetrad REE patterns. *Journal of Asian Earth Sciences*, **23**, 731–744.
Yin, C-J., Lu, X-P., Chen, Y-J., and Ji, C-H. (1999): Report of regional geological survey. *Institute of Regional Geological Survey of Jilin Province*, pp 29–33.
Zhang, J.-F. (1997): A preliminary study on the paleosuture zone between the Xingkai and Bohai Blocks in the Yanbian area. *Jilin Geology*, **16**, 30–37. (in Chinese with English abstract).